

# Stability domains for time-delay feedback control with latency

Philipp Hövel\* and Joshua E. S. Socolar

*Department of Physics and Center for Nonlinear and Complex Systems,  
Duke University, Durham, NC 27708*

(Dated: November 15, 2018)

We generalize a known analytical method for determining the stability of periodic orbits controlled by time-delay feedback methods when latencies associated with the generation and injection of the feedback signal cannot be ignored. We discuss the case of extended time-delay autosynchronization (ETDAS) and show that nontrivial qualitative features of the domain of control observed in experiments can be explained by taking into account the effects of both the unstable eigenmode and a single stable eigenmode in the Floquet theory.

## I. INTRODUCTION

Throughout the last decade the use of time delayed signals for controlling unstable periodic orbits (UPOs) has been a field of increasing interest. A method first introduced by Pyragas [1], known as “time-delay autosynchronization” (TDAS), calculates the control force from the difference of the current state to the state one period in the past. Socolar et al.[2] have shown that this technique can be improved by using states further in the past. This generalization of TDAS is called “extended time-delay autosynchronisation” (ETDAS). One great advantage of ETDAS over conventional feedback controller schemes is that it can be applied to high frequency oscillators. Since it employs a direct comparison of continuous signals generated by the system itself the only factors limiting the speed of the controller is the bandwidth of the amplifiers and signal propagation times. There is no need to generate a reference signal independently.

Experiments on electronic oscillators have shown that ETDAS can be effective [3]. They also show, however, that the latency time associated with signal propagation – the time required to compare the the current signal with its time delayed counterpart and inject the feedback into the system – can have important effects. Just [4] has shown how longer latency times decrease the range of feedback gains over which control is achieved for simple systems controlled by TDAS. Here we extend his analytic formalism, which consists of a first-order perturbation theory in the gain, to ETDAS and note some novel features of the behavior of the individual Floquet multipliers. We then show how the theory provides a qualitative explanation of the shape of the domain of control observed in the experiments of Sukow et al.[3].

## II. SYSTEM EQUATIONS AND PERTURBATION THEORY

In this section we review the formalism developed by Just, generalizing to the case of ETDAS controllers. We use the same notation as Bleich and Socolar [5] for the system equations and feedback signal, and the notation of Just [4] for the Floquet theory parameters.

Consider a  $N$ -dimensional dynamical system defined by

$$\dot{\mathbf{x}}(t) = \mathbf{f}(\mathbf{x}(t), \epsilon_0 + \epsilon(t)), \quad (1)$$

where  $\mathbf{x}(t)$  denotes a  $N$ -dimensional state vector,  $\epsilon_0$  is a parameter that can be modulated to achieve control, and  $\epsilon$  is a feedback signal. Assume that in the absence of control,  $\epsilon(t) = 0$ , there exists an unstable periodic orbit  $\mathbf{x}_0(t)$  with period  $\tau$ . Let  $\xi(t) = \hat{\mathbf{n}} \cdot \mathbf{x}(t)$  be a component of  $\mathbf{x}$  that can be continuously measured. The ETDAS feedback signal can be written in several equivalent forms:

$$\epsilon(t) = \gamma \sum_{k=1}^{\infty} R^k [\xi(t - t_l - k\tau) - \xi(t - t_l - (k+1)\tau)]$$

---

\*Permanent address: Institut für Theoretische Physik, TU Berlin, Hardenbergstrasse 36, D-10623 Berlin, Germany

$$\begin{aligned}
&= \gamma \left( \xi(t - t_l) - (1 - R) \sum_{k=1}^{\infty} R^{k-1} \xi(t - t_l - k\tau) \right) \\
&= \gamma (\xi(t - t_l) - \xi(t - t_l - \tau)) + R\epsilon(t - \tau),
\end{aligned} \tag{2}$$

where  $\gamma$  (the feedback gain) and  $R \in (-1, 1)$  are real parameters, and  $t_l$  is the latency time. The control force vanishes if the UPO is stabilized, since  $\xi(t - k\tau) = \xi(t)$  for all  $t$  and any integer  $k$ . TDAS corresponds to the special case  $R = 0$ . The last form is the basis for simple implementation of ETDAS in experiments.

In order to determine whether the controlled orbit is stable, Equation (1) is linearized around the UPO. Defining  $\mathbf{y}(t) = \mathbf{x}(t) - \mathbf{x}_0(t)$ , we have

$$\begin{aligned}
\dot{\mathbf{y}}(t) &= \mathbf{J}(t) \cdot \mathbf{y}(t) + \epsilon(t) \left. \frac{\partial \mathbf{f}}{\partial \epsilon} \right|_{\mathbf{x}_0(t), \epsilon=0} \\
&= \mathbf{J}(t) \cdot \mathbf{y}(t) + \gamma \mathbf{M}(t) \cdot \left( \mathbf{y}(t - t_l) - (1 - R) \sum_{k=1}^{\infty} R^{k-1} \mathbf{y}(t - t_l - k\tau) \right),
\end{aligned} \tag{3}$$

where  $\mathbf{J}(t) = \mathbf{J}(t)|_{\mathbf{x}_0(t), \epsilon=0}$  denotes the Jacobian matrix of the uncontrolled system, and  $\mathbf{M}(t) = \left. \frac{\partial \mathbf{f}}{\partial \epsilon} \right|_{\mathbf{x}_0(t), \epsilon=0} \otimes \hat{\mathbf{n}}$  is a  $N \times N$  matrix containing all information about the control force.

Since  $\mathbf{J}(t)$  and  $\mathbf{M}(t)$  are both periodic with period  $\tau$ , Floquet theory ensures that  $\mathbf{y}(t)$  can be written as

$$\mathbf{y}(t) = \sum_{m=0}^{\infty} \sum_{n=1}^N c_m^{(n)} e^{(\Lambda_m^{(n)} + i\Omega_m^{(n)})t} \mathbf{p}_m^{(n)}(t), \tag{4}$$

where  $\mathbf{p}_m^{(n)}(t)$  is a periodic function with period  $\tau$ :

$$\mathbf{p}_m^{(n)}(t) = \mathbf{p}_m^{(n)}(t + \tau). \tag{5}$$

The factorization of the sum into a double sum is done for convenience in the discussions below. In the absence of control, i.e. the absence of time delay terms, there are  $N$  eigenmodes of the system, indexed by  $n$ . When control is turned on, each of these gives rise to a countably infinite set of eigenmodes indexed by  $m$ . For each set, there is one eigenvalue that begins at the original value  $\lambda^{(n)} + i\omega^{(n)}$  for  $\gamma = 0$  and varies as  $\gamma$  is increased. The remaining members all have eigenvalues that approach either  $\log |R|/\tau$  or  $-\infty$  as  $\gamma$  approaches 0.

$\Lambda_m^{(n)}$  and  $\Omega_m^{(n)}$  are the real and imaginary parts of the Floquet exponent corresponding to the eigenmode  $\mathbf{p}_m^{(n)}(t)$ . Inserting Equation (4) into Equation (3) will lead to conditions that must be satisfied by  $\Lambda_m^{(n)}$  and  $\Omega_m^{(n)}$ . The system is linearly stable if and only if all  $\Lambda_m^{(n)}$  that satisfy these conditions are negative. Equations (3) and (4) yield the following equation for each of the modes  $\mathbf{p}_m^{(n)}(t)$ , where we drop the subscript  $m$  and superscript  $n$  for notational convenience:

$$(\Lambda + i\Omega)\mathbf{p}(t) + \dot{\mathbf{p}}(t) = \mathbf{J}(t)\mathbf{p}(t) + \gamma \mathbf{M}(t) e^{-(\Lambda + i\Omega)t_l} \frac{1 - e^{-(\Lambda + i\Omega)\tau}}{1 - R e^{-(\Lambda + i\Omega)\tau}} \mathbf{p}(t - t_l). \tag{6}$$

This equation is equivalent to

$$(\Lambda + i\Omega)\mathbf{p}(t; \kappa) + \dot{\mathbf{p}}(t; \kappa) = [\mathbf{J}(t) + \kappa \mathbf{M}(t) \cdot \mathbf{W}(t, -t_l)] \cdot \mathbf{p}(t; \kappa), \tag{7}$$

where  $\mathbf{W}(t, \Delta t)$  is the propagator defined by  $\mathbf{p}(t; \kappa) = \mathbf{W}(t, \Delta t) \cdot \mathbf{p}(t - \Delta t; \kappa)$  and

$$\kappa \equiv \gamma e^{-(\Lambda + i\Omega)t_l} \frac{1 - e^{-(\Lambda + i\Omega)\tau}}{1 - R e^{-(\Lambda + i\Omega)\tau}}. \tag{8}$$

Since  $\kappa$  is proportional to  $\gamma$ , it can be loosely thought of as a measure of the strength of the control gain. One must keep in mind, however, that the value of  $\kappa$  is ultimately determined by the solutions for the exponent  $\Lambda + i\Omega$ . Note also that the Floquet eigenmodes  $\mathbf{p}(t; \kappa)$  themselves depend on  $\Lambda + i\Omega$  through  $\kappa$ , making for a nontrivial modification of the usual eigenvalue problem.

An expression taking the effects of control into account can be derived by perturbation theory. Equation (7) can be written as

$$(\Lambda + i\Omega)\mathbf{p}(t; \kappa) = \left( -\frac{d}{dt} + \mathbf{J}(t) + \kappa \mathbf{M}(t) \cdot \mathbf{W}(t, -t_l) \right) \cdot \mathbf{p}(t; \kappa)(t). \tag{9}$$

We regard  $-\frac{d}{dt} + \mathbf{J}(t)$  as an operator with known eigenvalues  $\lambda^{(n)} = i\omega^{(n)}$  and consider  $\kappa\mathbf{M}(t) \cdot \mathbf{W}(t, t_l)$  to be a perturbation, a technique familiar from quantum mechanics. The effects of the controller on the Floquet exponents can be expanded in powers of  $\kappa$  as

$$\Lambda + i\Omega = \lambda + i\omega + \chi(t_l)\kappa + o(\kappa^2), \quad (10)$$

where the coefficient  $\chi(t_l)$  is a complex valued function. Any effects of interactions between the Floquet modes enter only at  $\kappa^2$ . This is why it is convenient to index the modes by  $n$  and  $m$  for the purposes of first-order perturbation theory.

As mentioned above, Equation (10) has an infinite number of solutions for  $\Lambda$  and  $\Omega$  which approach  $\log|R|/\tau$  [6, 7] or minus infinity as the feedback gain  $\gamma$  goes to zero. This behavior arises from the essential singularity at  $\Lambda = \log|R|/\tau$  and the divergence at  $\Lambda = -\infty$ , the latter arising only due to the nonzero latency time.

Just [4] has shown how the coefficient  $\chi(t_l)$  can be calculated. Let  $\mathbf{u}(t) = \mathbf{p}(t; \kappa = 0)$  and  $\mathbf{v}^*(t)$  be the right and left Floquet eigenmode in the absence of control,  $\kappa = 0$ . Both are periodic with period  $\tau$ , i.e.  $\mathbf{u}(t) = \mathbf{u}(t + \tau)$  and  $\mathbf{v}^*(t) = \mathbf{v}^*(t + \tau)$ . Now let  $\hat{\mathbf{u}}(t) = \exp(i\omega t)\mathbf{u}(t)$  and  $\hat{\mathbf{v}}^*(t) = \exp(-i\omega t)\mathbf{v}^*(t)$ . These satisfy the equations

$$\begin{aligned} \lambda\hat{\mathbf{u}}(t) + \dot{\hat{\mathbf{u}}}(t) &= \mathbf{J}(t) \cdot \hat{\mathbf{u}}(t) \\ \lambda\hat{\mathbf{v}}^*(t) - \dot{\hat{\mathbf{v}}}(t) &= \hat{\mathbf{v}}^*(t) \cdot \mathbf{J}(t), \end{aligned} \quad (11)$$

with the boundary conditions:

$$\begin{aligned} \hat{\mathbf{u}}(t + \tau) &= e^{i\omega\tau}\hat{\mathbf{u}}(t) \\ \hat{\mathbf{v}}^*(t + \tau) &= e^{-i\omega\tau}\hat{\mathbf{v}}^*(t). \end{aligned} \quad (12)$$

The standard first-order perturbation theory result for the coefficient  $\chi(t_l)$  is

$$\chi(t_l) = e^{i\omega t_l} \rho(t_l), \quad (13)$$

where

$$\rho(t_l) = \frac{\int_0^\tau \hat{\mathbf{v}}^*(t)\mathbf{M}(t) \cdot \mathbf{W}(t, t_l)\hat{\mathbf{u}}(t)dt}{\int_0^\tau \hat{\mathbf{v}}^*(t)\hat{\mathbf{u}}(t)dt}. \quad (14)$$

Now  $\rho(t_l)$  depends on  $t_l$  only through  $\mathbf{W}$ , and since  $\mathbf{u}(t)$  is  $\tau$ -periodic,  $\mathbf{W}(t, t_l + \tau)\mathbf{u}(t) = \mathbf{W}(t, t_l)\mathbf{u}(t)$ . Therefore,  $\rho(t_l)$  has to satisfy

$$\rho(t_l + \tau) = e^{i\omega\tau}\rho(t_l). \quad (15)$$

Inserting Equation (13) in Equation (10) and neglecting second order terms yields

$$\Lambda + i\Omega = \lambda + i\omega + \rho(t_l)\gamma e^{-(\Lambda+i(\Omega-\omega))t_l} \frac{1 - e^{-(\Lambda+i\Omega)\tau}}{1 - R e^{-(\Lambda+i\Omega)\tau}}. \quad (16)$$

Following the treatment of Just [4] for the  $R = 0$  case, we note that this expression can be simplified in the case of a so-called flip orbit, where  $\omega = \pi/\tau$ . Defining the frequency deviation  $\Delta\Omega = \Omega - \pi/\tau$ , Equation (16) can be rewritten as

$$\Lambda + i\Delta\Omega = \lambda + \rho(t_l)\gamma e^{-(\Lambda+i\Delta\Omega)t_l} \frac{1 + e^{-(\Lambda+i\Delta\Omega)\tau}}{1 + R e^{-(\Lambda+i\Delta\Omega)\tau}}. \quad (17)$$

Moreover, since all coefficients in Equation (11) are real, and for  $\omega = \pi/\tau$  the boundary conditions of Equation (12) are invariant under complex conjugation,  $\hat{\mathbf{u}}(t)$  and  $\hat{\mathbf{v}}^*(t)$  can always be chosen to be real valued. From Equation (14) it is then clear that  $\rho(t_l)$  is real and from Equation (15) we have  $\rho(t_l) = -\rho(t_l + \tau)$ .

We emphasize that  $\hat{\mathbf{u}}(t)$ ,  $\hat{\mathbf{v}}^*(t)$ , and  $\rho(t_l)$  are also real valued in the case of zero torsion, i.e.  $\omega = 0$ . In this case,  $\chi(t_l) = \rho(t_l)$  and  $\rho$  is  $\tau$ -periodic:  $\rho(t_l) = \rho(t_l + \tau)$ . For torsion-free perturbations, Equation (16) becomes

$$\Lambda + i\Omega = \lambda + \chi(t_l)\gamma e^{-(\Lambda+i\Omega)t_l} \frac{1 - e^{-(\Lambda+i\Omega)\tau}}{1 - R e^{-(\Lambda+i\Omega)\tau}}. \quad (18)$$

Although a nonzero torsion of all unstable eigenmodes is a necessary condition for possible control, [8] the case of  $\lambda < 0$  and  $\omega = 0$  might be interesting because an initially stable eigenmode can become unstable when the control force is applied and thus limit the domain of control.

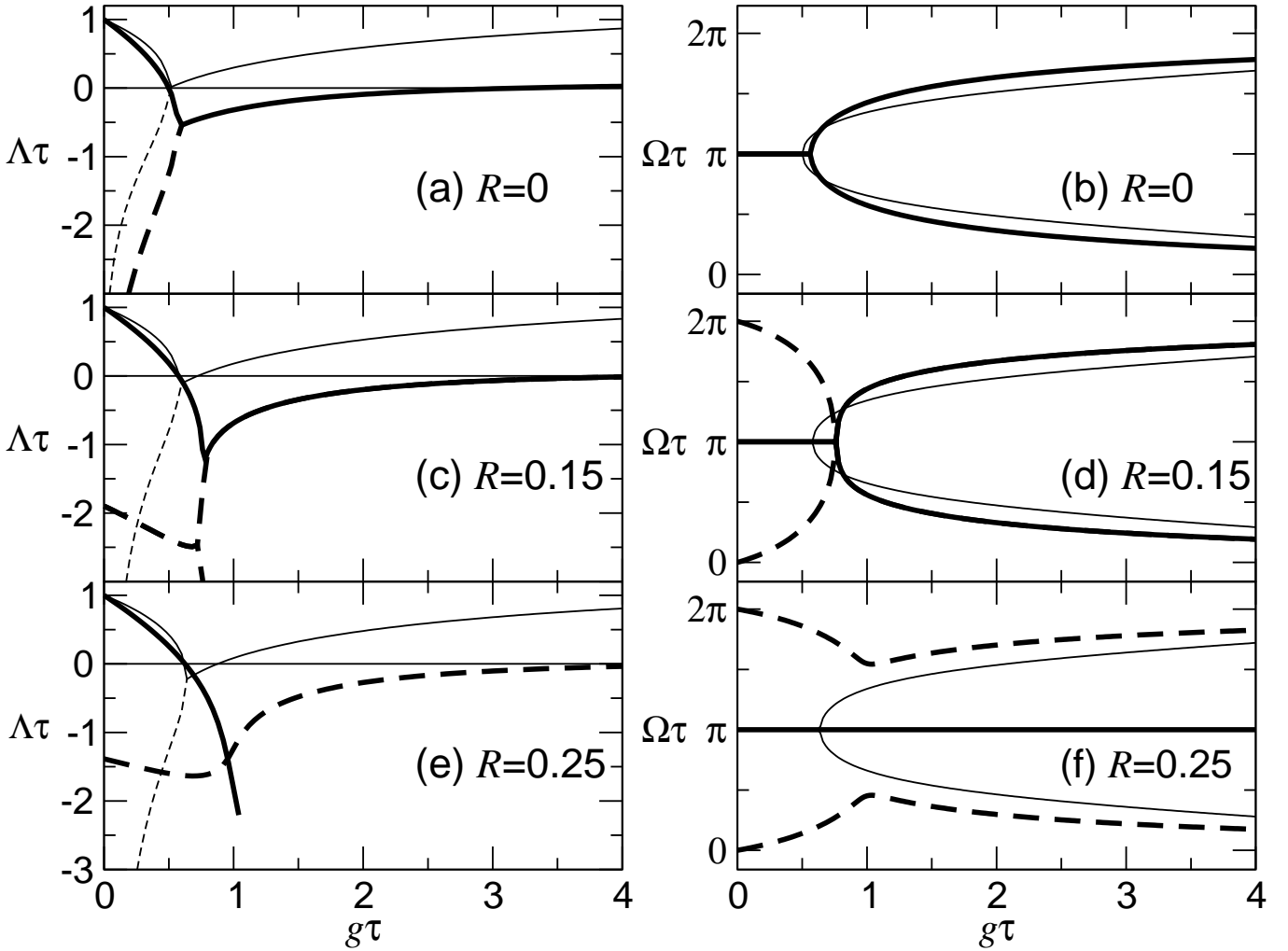


FIG. 1: Real and imaginary part of the Floquet exponent versus  $g$  for  $\lambda\tau = 1$ . Thick lines correspond to a latency time  $t_l = 0$ , thin lines to  $t_l = 0.5\tau$  for different values of  $R$ : 0 (TDAS), 0.15, 0.25. The solid line represents the system's exponent, the dashed line represents the exponent created by the control scheme.

### III. FLOQUET EXPONENTS FOR FIXED LATENCY TIME

To understand the solutions to Equation (17), it is helpful to first consider their behavior for fixed values of  $g \equiv -\rho(t_l)\gamma$ . A detailed discussion of the effects of variations of  $\rho$  with  $t_l$  will be presented in section IV.

The behavior of the real and imaginary parts of the Floquet exponent in Equation (17) can be seen in Figure 1. In each panel, curves are shown for both  $t_l = 0$  (thick lines) and  $t_l = \tau/2$  (thin lines). For  $g = 0$  (no control), the real part  $\Lambda$  is equal to  $\lambda$ . For increasing  $g$  the value of  $\Lambda$  decreases, reaching 0 at  $g = \lambda(1 + R)/2$ , then changing its sign; thus the orbit becomes stable. Further increase of  $g$  usually leads to a collision with an exponent created by the control scheme, forming a complex conjugate pair (see Figure 1(b), (d), and (f), except for the thick line in (f)). After the collision,  $\Lambda$  then begins to increase (see Figure 1(a), (c), and (e), except for the thick line in (e)). For  $g$  sufficiently large,  $\Lambda$  becomes positive again and control is lost.

Note that as  $g$  increases from zero, an infinite number of solutions to Equation (17) emerge from  $\log|R|/\tau$  as complex conjugate pairs. [6, 7] In order to collide with the single exponent coming from  $(\lambda + i\omega)\tau$ , one pair has to become real and separate (see Figure 1(d)). If this does not happen, a crossing of branches can occur. After the crossing, the complex conjugate pair becomes the branch with largest  $\Lambda$  and thus responsible for the stability of the system (see thick lines in Figure 1(e) and 1(f)).

Figure 1 illustrates that increasing the latency time  $t_l$  and/or decreasing  $R$  leads to a smaller range of  $g$  for successful control. In fact, one can compute a maximum latency time  $t_{max}$  for which control can be achieved, which corresponds to the case where the collision of the two branches occurs at  $\Lambda = 0$  as in the thin line in Figure 1(a). Using the

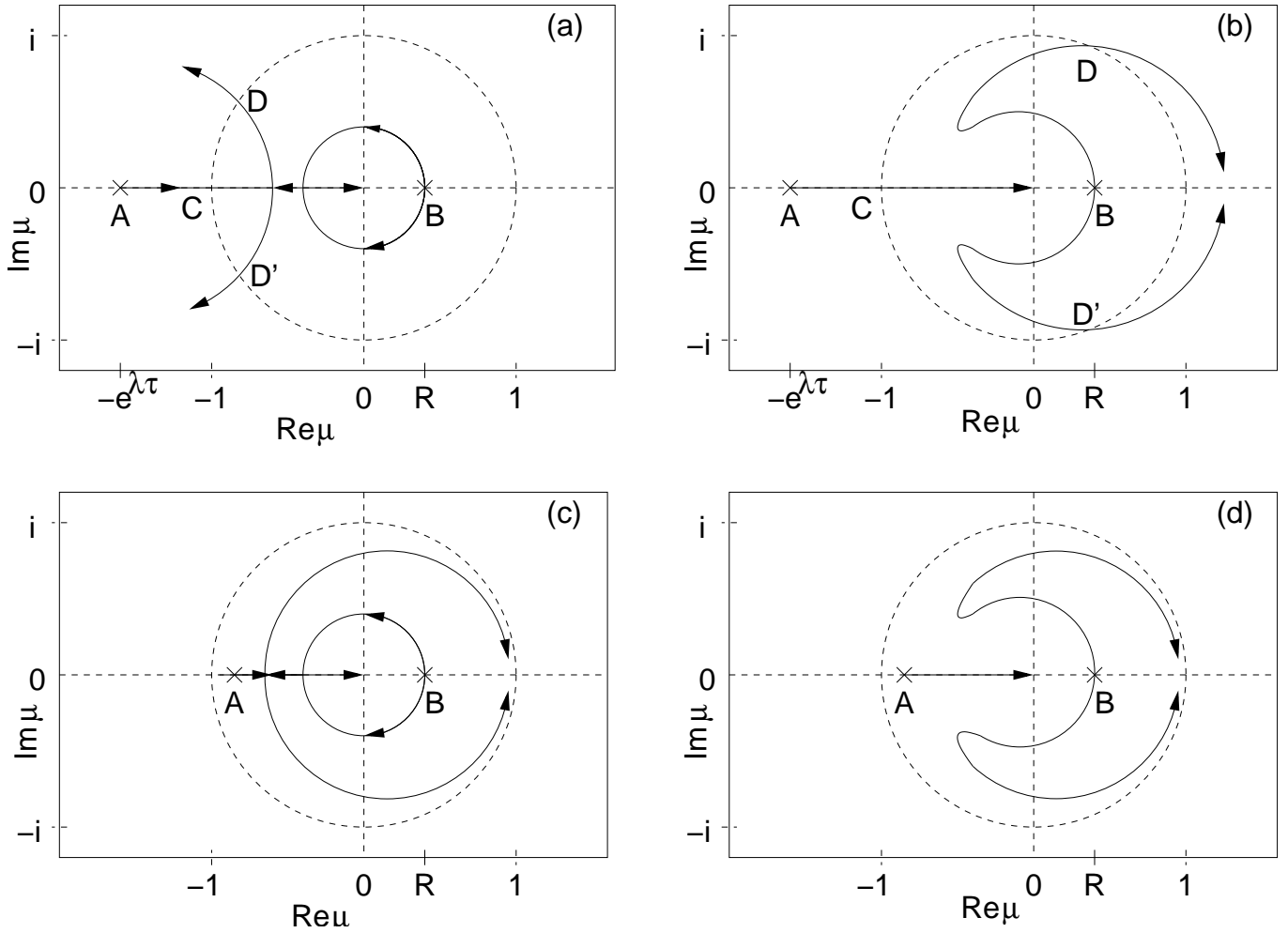


FIG. 2: Schematic behavior of the multiplier  $\mu$  in the complex plane for  $g > 0$  and  $t_l = 0$  in the case  $\omega = \pi/\tau$ . Pictures (a) and (b) visualize the case of an initially unstable multiplier of the system, pictures (c) and (d) the case of an initially stable one. Point A indicates the uncontrolled multiplier of the system  $\mu = -\exp(\lambda\tau)$ , point B shows where the created multipliers start, point C is the point where control is obtained, and points D and D' are the points where control is lost. The arrows indicate the directions in which the multipliers move for increasing  $g$ .

imaginary part of Equation (17) to eliminate the factor of  $g$  in the real part of that same equation and setting  $\Lambda$  equal to zero, one has to search for nontrivial solutions for  $\Delta\Omega$ . A condition for the existence of such a solution is

$$t_l \leq t_{max} = \frac{1}{\lambda} + \frac{\tau}{2} \frac{R-1}{R+1}. \quad (19)$$

This agrees with the result of [4] for  $R = 0$ . For larger latency time, control is not possible to first-order in  $\kappa$ . Equation (19) shows that negative  $R$  decreases the maximum latency time. We therefore focus on  $R \geq 0$  from here on.

Another way to visualize the effects of the control scheme is to consider how the Floquet *multipliers* (as opposed to exponents) evolve with varying  $g$ . We consider again the case  $\omega = \pi/\tau$ . The Floquet multipliers are defined by  $\mu_m^{(n)} = e^{(\Lambda_m^{(n)} + i\Delta\Omega_m^{(n)})\tau}$ . Dropping the subscript  $m$  and the superscript  $n$ , Equation (17) can be rewritten:

$$\mu = \exp \left[ \lambda\tau - g\tau \left( \frac{\mu+1}{\mu+R} \right) \mu^{-t_l/\tau} \right]. \quad (20)$$

Stability is achieved if all multipliers satisfy  $|\mu| < 1$ ; i.e. the multipliers  $\mu$  are located inside the unit circle in the complex plane.

Considering the real and imaginary part of Equation (20) and numerically following the roots of each equation in

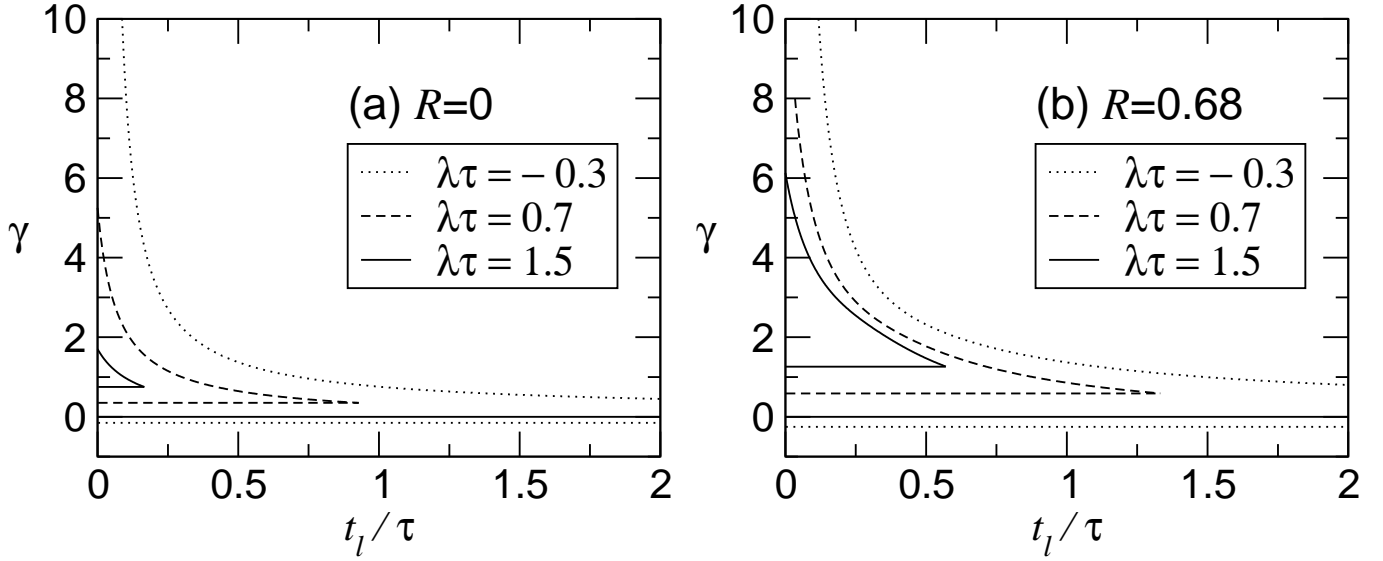


FIG. 3: Domain of control in the  $t_l$ - $\gamma$  plane for different values for  $\lambda\tau$ : -0.3, 0.7, 1.5 and  $\rho(t_l) = -1$ . Picture (a) shows the case of TDAS,  $R = 0$ , and picture (b) the case of  $R = 0.68$ . The branches indicate combinations for  $t_l$  and  $\gamma$  for which the real part of the Floquet exponent  $\Lambda$  changes sign and thus stability.

the complex plane (using Mathematica), we observe topologically different cases depending on the signs of  $\lambda$  and  $g$  in the absence of latency,  $t_l = 0$ , as illustrated in Figure 2.

- $g > 0; \lambda > 0$ : (Figure 2(a) and (b)) As  $g$  increases, the largest Floquet multiplier starts outside the unit circle at  $-\exp(\lambda\tau)$  on the real axis indicated by point A, moves towards the unit circle, and eventually crosses it. Meanwhile an infinite number of complex conjugate pairs spread out from  $\mu = R$  indicated by point B one of which will determine the stability range. Two scenarios are possible. One possibility is that one pair recombines on the real axis and one of the multipliers collides with the system's while the other approaches zero. After the collision they form a complex conjugate pair and cross the unit circle again (see Figure 2(a)). The other possibility is that the created pair becomes the largest multiplier, turns around and crosses the unit circle (see Figure 2(b)). The first case corresponds to the thick lines in Figure 1(c) and (d), the second to Figure 1(e) and (f).
- $g > 0; \lambda < 0$ : (Figure 2(c) and (d)) Similar to the previous case the largest Floquet multiplier starts at  $-\exp(\lambda\tau)$  on the real axis, this time inside the unit circle. It moves towards the origin for increasing  $g$  and may either collide with a multiplier created by the control force as in Figure 2(c), or continue towards zero while a complex conjugate pair becomes the largest multiplier as in Figure 2(d). In both cases all multipliers stay inside the unit circle for increasing  $g$ ; for  $\lambda < 0$  the system is stable for all  $g > 0$ .
- $g < 0; \lambda > 0$ : The largest multiplier starts at  $-\exp(\lambda\tau)$  on the real axis and goes to  $-\infty$ , thus control is never successful. All other multipliers created by the control scheme stay inside the unit circle for decreasing  $g$ .
- $g < 0; \lambda < 0$ : The largest multiplier starts inside the unit circle, crosses it, and goes to  $-\infty$ . More multipliers created by the control scheme cross the unit circle for further decrease of  $g$ .

#### IV. SHAPES OF THE DOMAIN OF CONTROL IN THE $t_l$ - $\gamma$ PLANE

For a discussion of the domain of control in the  $t_l$ - $\gamma$  plane let us consider first  $\rho(t_l) = -1$ . We will show later how the coefficient  $\rho(t_l)$  scales the domain at every value of the latency time.

For each  $\lambda$ , the lower branch in Figure 3 is the horizontal line  $\gamma = \lambda(1+R)/2$ , where there is a flip instability associated with the real exponent originating from  $\lambda$  at  $\gamma = 0$ . The upper branch corresponds to a Hopf bifurcation that can arise in two different ways: (1) the relevant complex conjugate pair of exponents originates in a collision between the branch associated with  $\lambda$  and a real eigenvalue created by the feedback scheme, as in Figure 1(a) or (c);

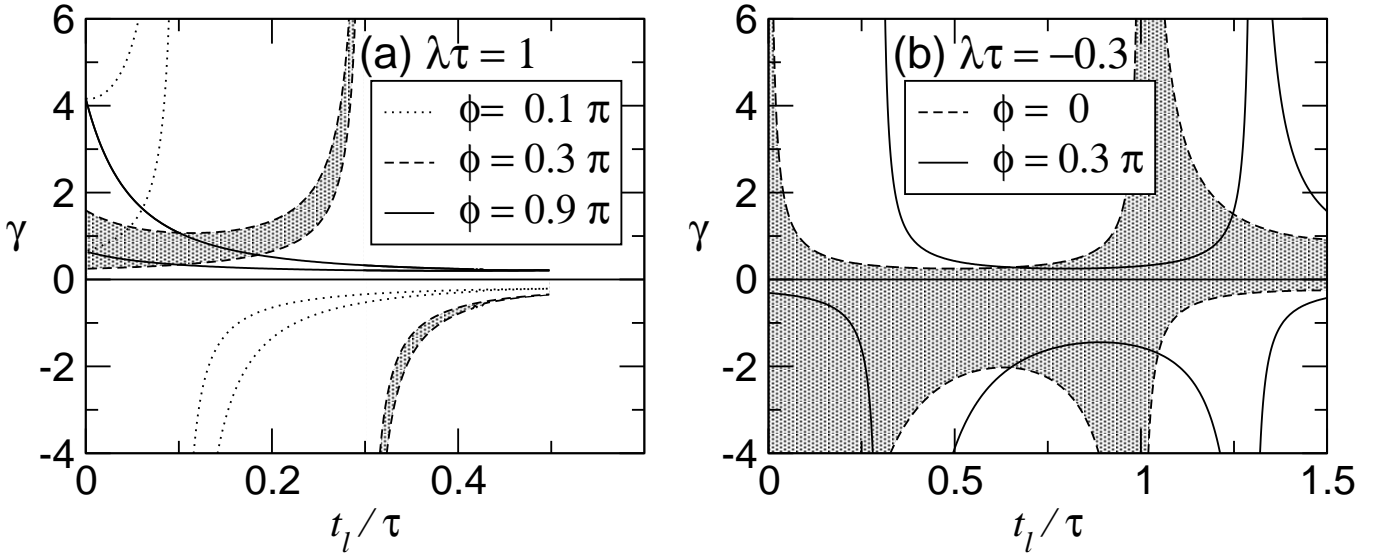


FIG. 4: Domain of control in the  $t_l$ - $\gamma$  plane for  $R = 0$  in case of  $\rho(t_l) = A \sin(\frac{\pi}{\tau}t_l - \phi)$ . Picture (a) shows the case of an UPO ( $\lambda\tau = 1$ ) with  $A = 2.5$  for different values of the phase  $\phi$ :  $0.1\pi, 0.3\pi, 0.9\pi$ . Picture (b) shows the case of a stable orbit ( $\lambda\tau = -0.3$ ) with  $A = 0.6$  for  $\phi$ :  $0, 0.7\pi$ . The shaded regions show the domain of stability for  $\phi = 0.3\pi$  and  $\phi = 0$ , respectively.

or (2) the relevant complex conjugate pair originates at  $\log |R|/\tau$ , as in the thick lines in Figure 1(d). It can be seen that increasing  $R$  and decreasing  $\lambda$  increases the domain of control at fixed  $t_l$  and increases  $t_{max}$  (see Equation (19)). The upper and lower curves do not intersect if the system is already stable, i.e.  $\lambda < 0$ .

The actual domain of control is a distortion of Figure 3 owing to the variation of  $\rho$  with  $t_l$ . The distortion is simple to compute, however, since changing the value of  $\rho$  is entirely equivalent to changing  $\gamma$ . Thus the values of  $\gamma$  on the upper and lower curves at a particular value of  $t_l$  are simply multiplied by  $-1/\rho(t_l)$ . Note that these variations in  $\rho$  cannot change the *ratio* of the upper and lower values of  $\gamma$ .

For eigenmodes with  $\omega = \pi/\tau$ , the antiperiodicity of  $\rho(t_l)$  and the fact that  $\rho(t_l)$  is real require that  $\rho(t_l)$  has at least one root in the interval  $[0, \tau]$ . We assume for convenience a sinusoidal form  $\rho(t_l) = A \sin(\frac{\pi}{\tau}t_l - \phi)$ . Figure 4 shows the domain of control for different values of the phase  $\phi$ . In each panel, the shading indicates the stable domain for one choice of  $\phi$ .

If a root of  $\rho(t_l)$  appears before the upper and lower branches intersect, the domain of control will include a region with negative feedback gain  $\gamma$ , as shown in Figure 4(a). Since the domain of control at fixed  $t_l$  scales like  $1/\rho$ , divergences appear at the values of the latency time for which  $\rho(t_l)$  vanishes. For  $\lambda < 0$ , shown in Figure 4(b), the upper and lower branches still do not intersect.

The case  $\lambda < 0$  can be important because it can reduce the domain of control, as shown in Figure 5(c) and (d), when the uncontrolled system has exponents  $\lambda_1 > 0$  and  $\lambda_2 < 0$ . Since second order terms are neglected in the perturbation theory, the different Floquet modes of the system do not interact with each other, so the effective domain of control is just the intersection of the single domains for each exponent.

Domains similar to those shown in Figure 5(c) and (d) have been observed in experiments on high speed diode resonator circuits. The analogous figure obtained from experiments is reproduced here as Figure 5(a) and (b) to facilitate comparison. To construct the theoretical figure, parameter values are adjusted to reproduce several features of the experimental results. From the experiments, three parameters are known: the weighting parameter  $R$ , the largest Lyapunov exponent  $\lambda_1$ , and, since the instability is a flip, the frequency  $\omega_1 = \pi/\tau$ . Equation (19) for the  $\lambda_1$  mode then gives an immediate prediction for  $t_{max}$ , the largest latency time for which control can be achieved. The agreement with the experiment is reasonable, especially given that the very narrow tails of the domains may be hard to detect in experiments.

We make the plausible assumption that the second largest Floquet mode is a stable flip, so  $\omega_2 = \pi/\tau$ . In our simple model, there are then five parameters that determine the shapes of the domains of control:  $\lambda_2\tau$  (the real part of the subleading exponent),  $A_1$  and  $A_2$  (the amplitudes of the variation in  $\rho_1$  and  $\rho_2$ ), and the phases  $\phi_1$  and  $\phi_2$  (which determine where  $\rho_1$  and  $\rho_2$  vanish).

To fix these five parameters, we consider the  $R = 0.68$  domain. The phase  $\phi_1$  must lie somewhere between  $t_1\pi$  and  $t_2\pi$  in order for the divergence in  $1/\rho$  and associated sign change in the domain of control to be right. From the fact that the onset of divergence is not evident yet at  $t_1$ , we estimate that  $\phi_1$  is close to  $t_2\pi$  and fix it at  $0.6\pi$ . From

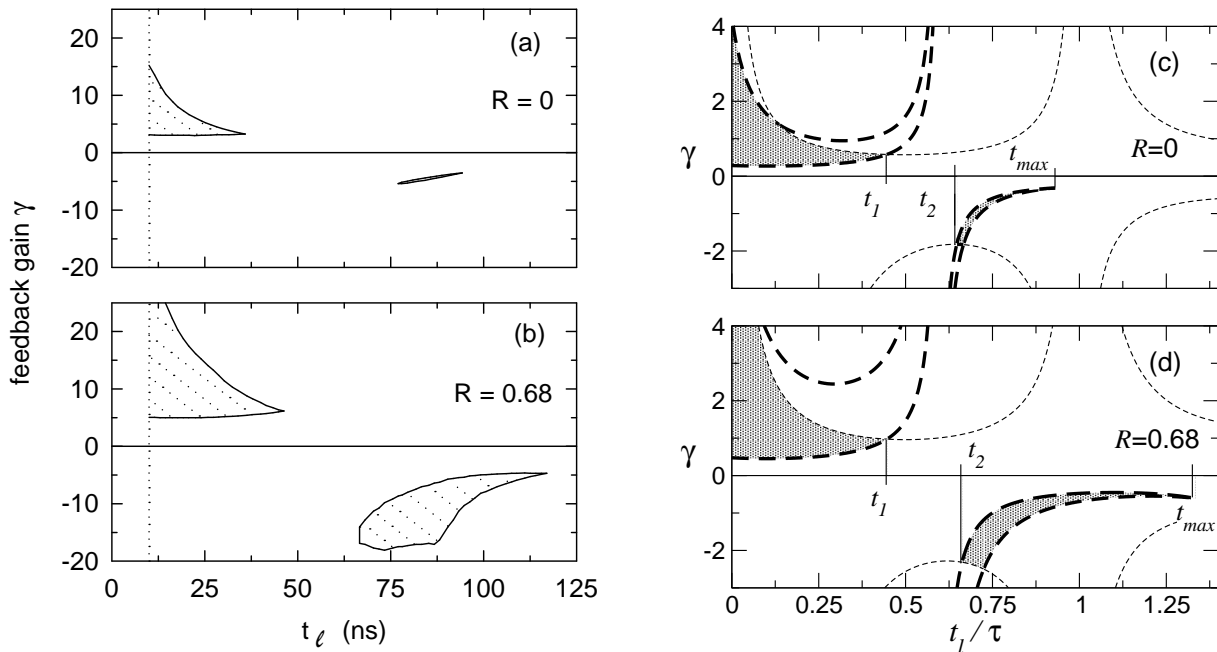


FIG. 5: Domain of control in the  $t_l$ - $\gamma$  plane. (a) and (b): Experimental result from a diode resonator circuit investigated by Sukow et al. This is a reproduction of Figure 18 from [3]. In this system, the period  $\tau$  was equal to 100 ns. The scale for the gain is multiplied by an arbitrary factor. (c) and (d): Domains determined from theory for two Floquet exponents with parameters chosen to reproduce as closely as possible the experimental results of (a) and (b). The thick and thin dashed lines show the domains corresponding to the two different modes. (See Figure 4.) The shaded regions show the combined domain of control. The parameter values are  $\lambda_1\tau = 0.7$ ,  $\lambda_2\tau = -1.6$ ,  $\omega_1 = \omega_2 = \pi/\tau$ ,  $\rho_1(t_l) = 1.3 \sin(\frac{\pi}{\tau}t_l - 0.6\pi)$  and  $\rho_2(t_l) = 1.4 \sin(\frac{\pi}{\tau}t_l)$ . The two panels show different values of the control parameter  $R$ . The special latency times marked are used to determine the parameter values as explained in the text.

the fact that the boundary of the subleading mode does not appear to cut off the domain near  $t_l = 0$ , we take the divergence of  $\rho_2$  to occur there, requiring  $\phi_2 = 0$  or  $\pi$ . The remaining parameters,  $A_1$ ,  $A_2$ , and  $\lambda_2\tau$  are adjusted to fit  $t_1$ ,  $t_2$ , the latency times (in units of  $\tau$ ) corresponding to the limits of the domains, and  $\gamma(t_2)$ , the gain at which the lower domain of control is cut off at  $t_2$ . The parameters determined from the  $R = 0.68$  data are used for the  $R = 0$  plot as well since  $\rho(t_l)$  is determined purely from the uncontrolled system.

The primary conclusion we draw is that the theory does give qualitative insight into the structure of the stability domains. Even with our crude constraints on the form of  $\rho(t_l)$ , the general shapes of the domains are reproduced surprisingly well. As expected, larger  $R$  increases the size of the domain of control, especially the part with negative  $\gamma$ .

It may appear that by adjusting the full functions  $\rho_1$  and  $\rho_2$  one could fit arbitrary shapes of the stability domains, and it is true that many types of undulations in the domain boundaries could be fit. Moreover, one can always appeal to lack of robustness to noise to explain why very narrow regions of a predicted stability domain would not show up in the experimental data. There are, however, some features of the experimental data that cannot be reproduced by the theory presented here. In particular, consider the width of the region at negative  $\gamma$  for  $R = 0.68$ . The upper and lower boundaries of the right half of this region both represent instabilities in the same mode, the mode associated with  $\lambda_1$ . For a fixed value of  $t_l$ , then, the ratio of the  $\gamma$ 's at these boundaries is independent of  $\rho$ . The substantially larger width of the experimental stability domain cannot be obtained by adjusting any of the parameters in our theory. Including additional modes or making a different assumption about  $\omega_2$  would not help, since the narrowness of the theoretical domain is determined by  $\lambda_1$ . We therefore conclude that second-order effects are significant in the experimental system. These effects may involve interactions between modes associated with different  $\lambda$ 's or just interactions of modes within the set generated by  $\lambda_1$  alone.

Our analysis can also be used to explore the possibilities for qualitatively different domain shapes. An interesting example is obtained when  $\phi_2$ , the phase associated with the subleading mode of the uncontrolled system is taken to be  $0.1\pi$  (and  $A_2 < 0$ ). As shown in Figure 6, this can lead to a situation in which a nonzero latency time is *required* for effective control.



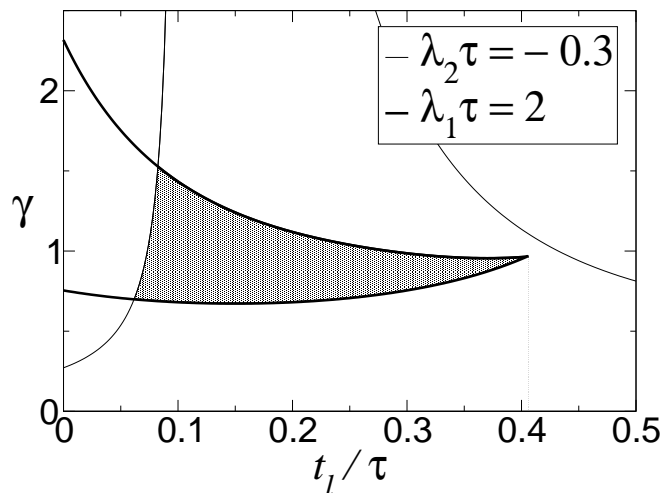


FIG. 6: Domain of control for two non-interacting Floquet modes,  $\lambda_1\tau = 2$ ,  $\lambda_2\tau = -0.3$ , and  $\omega_1 = \omega_2 = \pi/\tau$  for  $R = 0.68$ . The parameters  $\phi$  and  $A$  are chosen as  $\phi_1 = 0.65\pi$ ,  $A_1 = 2.5$  and  $\phi_2 = 0.1$ ,  $A_2 = -3$ . The shaded area is the effective domain of control.

## V. CONCLUSION

We have discussed the effects of latency time on a feedback control scheme known as ETDAS. Using Floquet theory and carrying out a first-order perturbation theory in the feedback gain, we have shown that nontrivial domain shapes can arise in the plane parameterized by feedback gain and latency time. Within the first order theory, we find that no control is possible above a maximum latency time determined solely by the Floquet exponent of the most unstable mode in the uncontrolled system. We also find that Floquet modes that are stable in the uncontrolled system contribute significantly to the overall stability picture, reducing the domain of control substantially.

The theory accounts well for qualitative features of the stability domains observed in experiments. As expected, larger values of the ETDAS parameter  $R$  give larger stability domains. Detailed comparison indicates, however, that second order effects are experimentally observable.

## Acknowledgments

We would like to thank E. Schöll, W. Just, A. Amann, I. Harrington, and D. Gauthier for useful conversations. This work was supported by NSF Grant PHY-98-70028 and within the framework of the exchange program between TU Berlin and Duke University. P.H. acknowledges a Fulbright Scholarship.

- 
- [1] K. Pyragas, Phys. Lett. A **170**, 421 (1992).
  - [2] J. E. S. Socolar, D. W. Sukow, and D. J. Gauthier, Phys. Rev. E **50**, 3245 (1994).
  - [3] D. W. Sukow, M. E. Bleich, D. J. Gauthier, and J. E. S. Socolar, Chaos **7**, 560 (1997).
  - [4] W. Just, D. Reckwerth, E. Reibold, and H. Benner, Phys. Rev. E **59**, 2826 (1999).
  - [5] M. E. Bleich and J. E. S. Socolar, Phys. Lett. A **210**, 87 (1996).
  - [6] K. Pyragas, Phys. Rev. Lett. **86**, 2265 (2001).
  - [7] O. Beck, A. Amann, E. Schöll, J. Socolar, and W. Just, Phys. Rev. E **66**, 016213 (2002).
  - [8] W. Just, T. Bernard, M. Ostheimer, E. Reibold, and H. Benner, Phys. Rev. Lett. **78**, 203 (1997).